BULLETIN OF THE EARTHQUAKE
RESEARCH INSTITUTE
Vol. 46 (1968), pp. 791-819

38. *Theoretical Seismograms of Spheroidal Type on the Surface of a Gravitating Elastic Sphere. III. Case of a Homogeneous Mantle with a Liquid Core.*

By Tatsuo USAMI, Yasuo SATÔ,
Earthquake Research Institute;
Mark LANDISMAN,
Geosciences Division, Southwest Center for Advanced Studies
and
Toshikazu ODAKA,
Geophysical Institute, the University of Tokyo.

(Read Nov. 28, 1967.—Received May 31, 1968.)

Abstract

Theoretical seismograms of spheroidal disturbances on the surface of an elastic sphere consisting of a homogeneous mantle and a liquid core are calculated when uniform radial stress is applied to a small circle around the pole. The effect of gravity is taken into consideration. Contributions are included from the free spheroidal oscillations of the first few radial modes for all orders with periods larger than 12 sec. The results of these computations are compared with the corresponding quantities for the case excluding the effect of gravity.

Noteworthy results from the study of spheroidal disturbances propagating on the surface of a gravitating elastic sphere with a homogeneous mantle and a liquid core, when the uniform radial stress is applied to a circular area around the pole, are:

1. The difference between non-dimensional frequency for the present case and for the case excluding the effect of gravity is not a simple function. The discrepancy is large for modes lying along the branch specified by $i=1'$; it tends toward negligible values as the order number increases.

2. The corresponding phase and group velocities exhibit their greatest differences for the first three radial modes and for orders less than about 15. The number of maxima and minima for the group velocity curves increases with radial mode number i. Curves connecting corresponding maxima and minima tend toward the value $U/V_{S0}\fallingdotseq 1.2$ as the period decreases to zero; in the case of the homogeneous sphere these curves approach 1.3.

(Contribution No. 79. Geosciences Division, Southwest Center for Advanced Studies)

3. The amplitudes of the Common Spectrum suggest that higher radial modes with $i \geq 10$ may still give appreciable contributions to the theoretical seismogram.

4. The Rayleigh wave shows a simple disturbance consisting of approximately one cycle of oscillation. The pattern of wave propagation can be explained by the concept of dispersion.

5. The convergence of the wave form of the P wave by the successive addition of radial higher modes is not so rapid as in the case without gravity. The slower convergence is caused by the difference of the time and space functions of the applied forces and by the minimum values of period employed in the synthesis.

6. The orbital motion of the Rayleigh wave shows a phase advance of $\pi/2$ near the antipode.

7. In the seismograms showing body waves, the surface-reflected S waves end abruptly near the travel time of a wave propagating along the surface with the shear wave velocity.

8. The variation of amplitude of the body waves as a function of epicentral distance can be explained by the theory of the divergence factor, after accounting for the effect of reflection at the surface.

1. Introduction

Theoretical seismograms of torsional and spheroidal disturbances have been calculated during the past few years for various cases from simple models such as the homogeneous elastic sphere[1] to realistic earth models under the influence of gravity[2]. Basic properties have been found which characterize the behavior of these theoretical seismograms. 1) The fundamental mode is closely related to the surface waves and the higher radial modes to the body waves. 2) The waves in the S group, which travel most of their paths as S waves, are well represented by contributions from the lower radial modes, while higher overtones are necessary to express the P wave group. 3) The apparent arrival times and amplitudes of body waves identified on the theoretical seismograms usually are concordant with values calculated from the

1) Y. SATÔ, T. USAMI and M. EWING, "Basic Study on the Oscillation of a Homogeneous Elastic Sphere IV. Propagation of Disturbances on the Sphere," *Geophys. Mag.*, **31** (1962), 237-242.

T. USAMI and Y. SATÔ, "Propagation of Spheroidal Disturbances on a Homogeneous Elastic Sphere," *Bull. Earthq. Res. Inst.*, **42**, (1964), 273-287.

2) Y. SATÔ, T. USAMI and M. LANDISMAN, "Theoretical Seismograms of Spheroidal Type on the Surface of a Gravitating Elastic Sphere. II. Case of Gutenberg-Bullen A′ Earth Model," *Bull. Earthq. Res. Inst.*, **45** (1967), 601-624.

theory of geometrical optics. 4) The introduction of the core causes special transition branches on the non-dimensional frequency vs. colatitudinal order number curves for the spheroidal oscillations. Spheroidal modes on these branches show features characteristic of boundary waves between two different media.

The effect of gravity on the propagation of spheroidal disturbances has been investigated for two cases, a homogeneous elastic sphere[3] and the Gutenberg-Bullen A′ earth model[2]. In these investigations, the effect of gravity on the non-dimensional frequencies was found to be complicated, but the resulting theoretical seismograms were not greatly altered.

The present study, the third one of the effect of gravity on the periods of free spheroidal oscillations, its effects on the phase and group velocities, Common Spectrum and on the theoretical seismograms was planned in order to unravel the influence of gravity and to make clear the extent of the contributions from various parameters. A homogeneous mantle and a liquid core were assumed. The theoretical seismograms representing the disturbances on the surface were calculated by summing up contribution from the free spheroidal oscillations through the tenth radial mode, for all orders from the gravest with period 55 minutes to those with periods near 12 seconds. Phase and group velocities, the Common Spectrum and theoretical seismograms were calculated and comparisons were made with the corresponding quantities found for the case excluding the effect of gravity. In the latter[4], the shortest periods employed in the synthesis were about 60 seconds. Special attention was paid to the propagation of Rayleigh waves and to the variation of wave form and orbital motion with epicentral distance, as these observable quantities are related to the polar phase shift.

2. Glossary

a: radius of the sphere
b: radius of the core
C, U: phase and group velocities
E_S, E_T: radial and colatitudinal components of stress on the surface

3) T. USAMI and Y. SATÔ, "Theoretical Seismograms of Spheroidal Type on the Surface of a Homogeneous Gravitating Spherical Earth," *Bull. Earthq. Res. Inst.*, **44** (1966), 779-791.

4) Y. SATÔ and T. USAMI, "Propagation of Spheroidal Disturbances on an Elastic Sphere with a Homogeneous Mantle and a Core," *Bull. Earthq. Res. Inst.*, **42** (1964), 407-425.

$f(t)$: time function of the applied force
$f^*(p)$: Fourier transform of the function $f(t)$
g_0: gravity in the undisturbed state
i: radial mode number
j: unit of the imaginary number
k: $(=p/V_{S0})$
m: degree of an associated Legendre function
n: order of an associated Legendre function
p: circular frequency
$P_n^m(\cos\theta)$: associated Legendre function by Ferrers' definition
(r, θ, φ): polar coordinates
${}_iS_n^u, {}_iS_n^v$: Common Spectrum of radial and colatitudinal components of disturbance
S_{mn}, T_{mn}: coefficients of spherical surface harmonics in the expansion of radial and colatitudinal components of applied force
S_r: wave propagated along the surface with the velocity of S waves
t: time
T, T_i: period
(u, v, w): displacement in the r-, θ-, and φ-directions
$U_n(r), V_n(r), Y_n(r)$: function giving radial distribution of u, v, and ψ
${}_iu_n, {}_iv_n$: contribution of a normal mode oscillation for the radial mode number i and the order number n
$({}_iu_n), ({}_iv_n)$: $\sum_{i'=1}^{i}\sum_{n'=0}^{n} {}_{i'}u_{n'}$, $\sum_{i'=1}^{i}\sum_{n'=0}^{n} {}_{i'}v_{n'}$
V_P, V_S: velocities of dilatational and shear waves
V_{S0}: S wave velocity on the surface of the sphere
β: phase angle at the source of ${}_iS_n^u \cdot P_n^m(\cos\theta)$ or ${}_iS_n^v \cdot \frac{d}{d\theta}P_n^m(\cos\theta)$
γ: universal constant of gravity
η: non-dimensional frequency of free oscillation
λ, μ: Lamé's elastic moduli
ρ_0: density in the undisturbed state
θ_0, θ_1: angle defined in Figure 9
ψ: gravitational potential due to disturbance
φ_u, φ_v: phase angle of radial and colatitudinal displacement defined in § 9
φ_c: $\varphi_u - \varphi_v$
$\Phi(\theta, \varphi)$: spatial distribution of external force

3. Fundamental Expressions

The spheroidal disturbance of a radially heterogeneous elastic sphere, when the effect of gravity is considered, may be expressed in the polar coordinates $(r,\ \theta,\ \varphi)$,

$$(u, v, w, \psi)=\frac{1}{2\pi}\int_{-\infty}^{\infty}(u(p), v(p), w(p), \psi(p)\cdot\exp(jpt)dp\ , \tag{3.1}$$

$$\left.\begin{aligned}
u(p)&=\sum_{m,n} A_{mn}U_n(r)\cdot P_n^m(\cos\theta)\cdot\begin{matrix}\cos\\ \sin\end{matrix} m\varphi\cdot f^*(p)\ ,\\
v(p)&=\sum_{m,n} A_{mn}V_n(r)\cdot\frac{d}{d\theta}P_n^m(\cos\theta)\cdot\begin{matrix}\cos\\ \sin\end{matrix} m\varphi\cdot f^*(p)\ ,\\
w(p)&=\sum_{m,n} A_{mn}mV_n(r)\cdot\frac{P_n^m(\cos\theta)}{\sin\theta}\cdot\begin{matrix}-\sin\\ \cos\end{matrix} m\varphi\cdot f^*(p)\ ,\\
\psi(p)&=\sum_{m,n} A_{mn}Y_n(r)\cdot P_n^m(\cos\theta)\cdot\begin{matrix}\cos\\ \sin\end{matrix} m\varphi\cdot f^*(p)\ ,
\end{aligned}\right\} \tag{3.2}$$

where u, v, w are the displacement components in the r-, θ-, φ-directions and ψ is the gravity potential due to the disturbances. U_n, V_n and Y_n, the radial distributions of displacement and gravity potential, satisfy the simultaneous differential equations,

$$\left.\begin{aligned}
&\frac{d}{dr}(\lambda X_n+2\mu\dot{U}_n)+\frac{\mu}{r^2}[4r\dot{U}_n-4U_n+n(n+1)(-U_n-r\dot{V}_n+3V_n)]\\
&\qquad+\rho_0\dot{Y}_n+\rho_0 g_0 X_n-\rho_0\frac{d}{dr}(g_0U_n)+\rho_0 p^2U_n=0\ ,\\
&\frac{d}{dr}\left[\mu\left(\dot{V}_n-\frac{V_n-U_n}{r}\right)\right]+\frac{\mu}{r^2}[5U_n+3r\dot{V}_n-V_n-2n(n+1)V_n]\\
&\qquad+\frac{\lambda}{r}X_n+\frac{\rho_0}{r}Y_n-\rho_0 g_0\frac{U_n}{r}+\rho_0 p^2V_n=0\ ,\\
&\ddot{Y}_n+\frac{2}{r}\dot{Y}_n-n(n+1)\frac{Y_n}{r^2}=4\pi\gamma(\dot{\rho}_0U_n+\rho_0X_n)\ ,\\
&X_n=\dot{U}_n+\frac{2}{r}U_n-n(n+1)\frac{V_n}{r}\ .
\end{aligned}\right\} \tag{3.3}$$

γ is the universal constant of gravitation and ρ_0 and g_0 are the density and gravity in the undisturbed state. A dot over a quantity implies differentiation with respect to the radius r.

Denoting the coefficients of spherical surface harmonics in the surficial expansion of the radial and tangential stresses applied on the surface by S_{mn} and T_{mn}, the displacement components in the time domain can be expressed, through the technique of contour integration, as

$$\left.\begin{aligned} u(t)&=\frac{j}{2}\sum_{i,m,n} P_n^m(\cos\theta)\cdot\begin{matrix}\cos\\ \sin\end{matrix} m\varphi\cdot\left[\left(\frac{S_{mn}}{dE_S/dp}+\frac{T_{mn}}{dE_T/dp}\right)\cdot U_n(r)\cdot f^*(p)\cdot\exp(jpt)\right]_{p=ip_n}\ ,\\ v(t)&=\frac{j}{2}\sum_{i,m,n}\frac{d}{d\theta}P_n^m(\cos\theta)\cdot\begin{matrix}\cos\\ \sin\end{matrix} m\varphi\cdot\left[\left(\frac{S_{mn}}{dE_S/dp}+\frac{T_{mn}}{dE_T/dp}\right)\cdot V_n(r)\cdot f^*(p)\cdot\exp(jpt)\right]_{p=ip_n}\ ,\\ w(t)&=\frac{j}{2}\sum_{i,m,n}\frac{m\cdot P_n^m(\cos\theta)}{\sin\theta}\cdot\begin{matrix}-\sin\\ \cos\end{matrix} m\varphi\cdot\left[\left(\frac{S_{mn}}{dE_S/dp}+\frac{T_{mn}}{dE_T/dp}\right)\cdot V_n(r)\cdot f^*(p)\cdot\exp(jpt)\right]_{p=ip_n}\ . \end{aligned}\right\} \tag{3.4}$$

E_S and E_T are the radial and tangential stress at the free surface $r=a$,

$$\left.\begin{aligned} E_S&=(\lambda+2\mu)_a\cdot\dot{U}_n(a)+\frac{(\lambda)_a}{a}\cdot(2U_n(a)-n(n+1)V_n(a))\ ,\\ E_T&=(\mu)_a\cdot\left(\dot{V}_n(a)-\frac{1}{a}(V_n(a)-U_n(a))\right)\ . \end{aligned}\right\} \tag{3.5}$$

$E_S=E_T=0$, together with the relation

$$\dot{Y}_n(a)+\frac{n+1}{a}Y_n(a)=4\pi\gamma\cdot(\rho_0)_a\cdot U_n(a)\ , \tag{3.6}$$

comprise the exterior surface boundary conditions for free spheroidal oscillations of a gravitating elastic sphere.

4. Earth Model

The earth model employed in our previous paper[4] was adopted here. However, when the effect of gravity is introduced, it is insufficient to specify the ratio of densities in the mantle and core; the absolute values of density are necessary in order to determine uniquely the natural periods of free spheroidal oscillation. Values of parameters characterizing the model are

$$a=6370 \text{ km},$$
$$b=(6370-2900) \text{ km},$$
$$\rho_i/\rho_0=2.2,$$
$$\rho_i=10.171, \quad \rho_0=4.6232,$$
$$V_{P0}=11.55 \text{ km/sec},$$
$$V_{S0}=V_{P0}/\sqrt{3}=6.667 \text{ km/sec},$$
$$V_{Pi}=10.00 \text{ km/sec}.$$

The above density values give 5.52 gr/cm^3 as the mean density of the model sphere, a value equal to the corresponding one for the actual earth.

5. Non-dimensional Frequency of Oscillation

The eigenfrequencies of the free spheroidal oscillations are obtained by solving the differential equations (3.3) under the boundary conditions:

1) Vanishing of the radial and tangential stresses and the continuity of the gravitational potential on the surface $r=a$ and

2) Continuity of the radial and tangential components of displacement and stress and the continuity of the gravitational potential and the gravitational force on the core boundary, $r=b$.

Since a model consisting of a homogeneous mantle and a liquid core is assumed in the present study, the functions U_n, V_n and Y_n can be expressed by the spherical Bessel functions. In the present study, however, the non-dimensional frequency of free spheroidal oscillation $\eta(=ka=pa/V_{S0})$ is calculated by numerically integrating the equation (3.3). The method was explained in a previous paper[2] which treated the case of a Gutenberg-Bullen A′ earth model.

The non-dimensional frequencies through the tenth radial mode, for all orders with periods longer than about 12 sec, were calculated and are arranged in Figures 1-a and 1-b together with those obtained for the case excluding the effect of gravity. As is physically reasonable, the difference between the non-dimensional frequencies, for the cases with and without the influence of gravity, becomes negligibly small as the colatitudinal order number n increases. The existence of the core has little effect on the free oscillations of short period. Therefore, the curves for large values of n represent nothing but the frequency for the case of a homogeneous elastic sphere. Modes on a special branch specified by $i=1'$ show large amplitudes near the core boundary, a

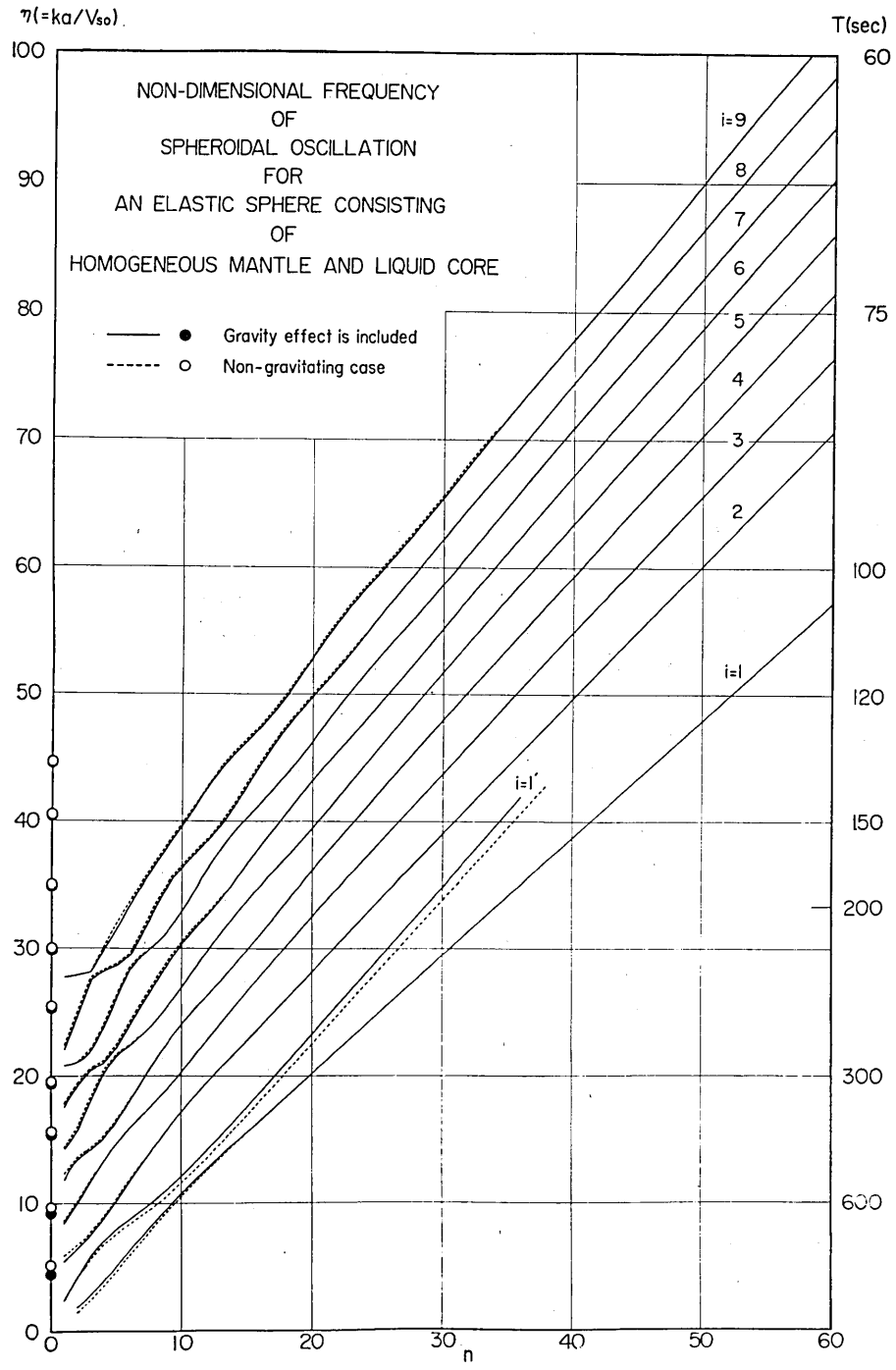
η(=ka/Vso)
T(sec)
NON-DIMENSIONAL FREQUENCY
OF
SPHEROIDAL OSCILLATION
FOR
AN ELASTIC SPHERE CONSISTING
OF
HOMOGENEOUS MANTLE AND LIQUID CORE
Gravity effect is included
Non-gravitating case
i=9
8
7
6
5
4
3
2
i=1
i=1'
n
100
90
80
70
60
50
40
30
20
10
0
60
75
100
120
150
200
300
600
0
10
20
30
40
50
60

Fig. 1-a.

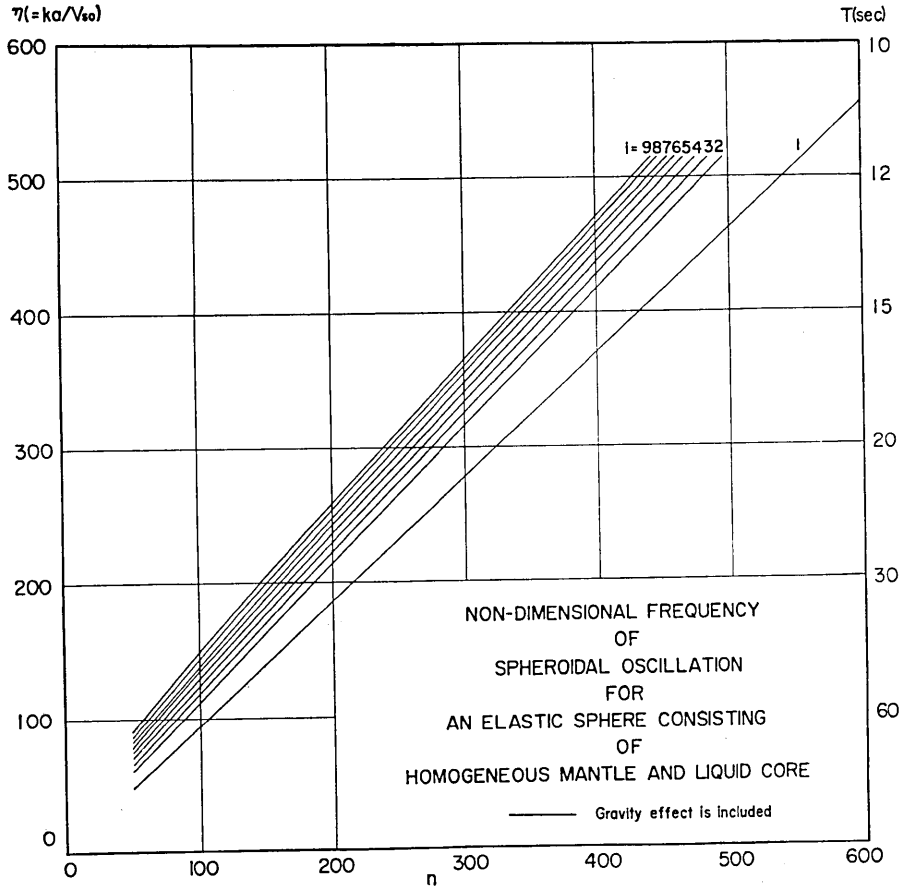

Fig. 1-b.

Fig. 1. Non-dimensional frequency $\eta(=ka/Vs_0)$ of spheroidal oscillation for an elastic sphere consisting of a homogeneous mantle and a liquid core. Solid lines and solid circles: case when the effect of gravity is included. Broken lines and open circles: case without influence of gravity. As the colatitudinal order number n increases, the difference between solid and broken lines becomes negligible. Fig. 1-a is reproduced from the preliminary report[5].

characteristic associated with Stoneley waves between two different media.

6. Phase and Group Velocities

Phase and group velocities are calculated from the non-dimensional

5) Y. SATÔ, T. USAMI and M. LANDISMAN, "Preliminary Report: Theoretical Seismograms Excited by a Localized Radial Stress on the Surface of a Gravitating Homogeneous Mantle over a Liquid Core," *Nuovo Cimento* (in print).

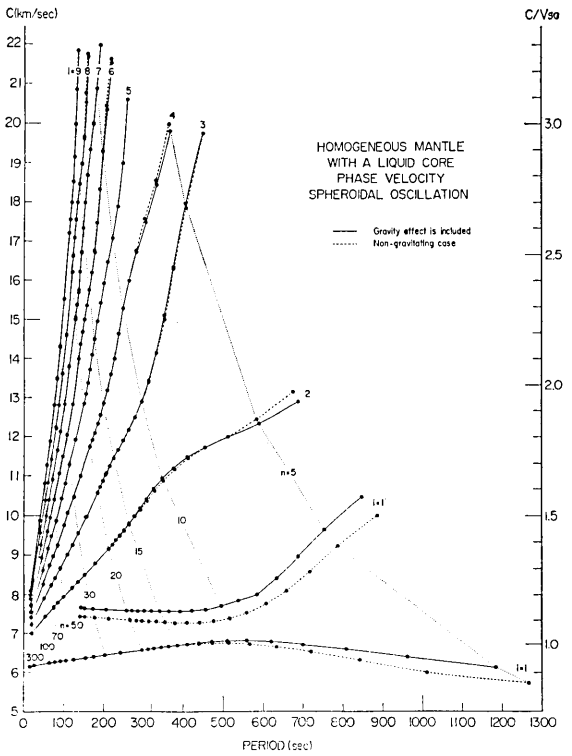
C(km/sec)
C/Vso
HOMOGENEOUS MANTLE
WITH A LIQUID CORE
PHASE VELOCITY
SPHEROIDAL OSCILLATION
Gravity effect is included
Non-gravitating case
PERIOD (sec)

Fig. 2-a.

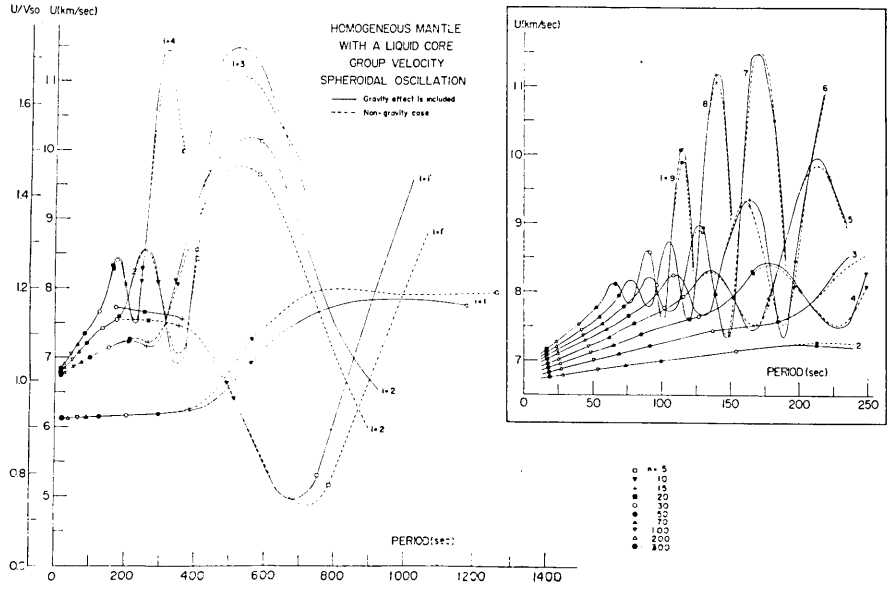
U/Vso U(km/sec)
HOMOGENEOUS MANTLE
WITH A LIQUID CORE
GROUP VELOCITY
SPHEROIDAL OSCILLATION
Gravity effect is included
Non-gravity case
PERIOD(sec)
U(km/sec)
PERIOD (sec)

Fig. 2-b.

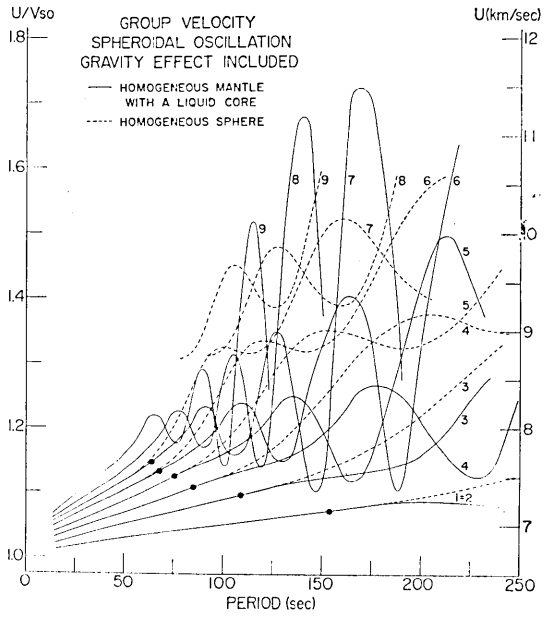

Fig. 2-c.

Fig. 2. Phase and group velocity as functions of period. Solid lines refer to the case of a gravitating elastic sphere and broken lines to the case without the effect of gravity. In the fundamental mode ($i=1$), the phase and group velocities both tend toward the corresponding value of a plane Rayleigh wave, 0.9194 Vs_0, as the period tends toward zero. In order to show the detailed features of group velocity, the short period part is enlarged in the rectangular enclosure. The group velocity of a homogeneous sphere and a homogeneous mantle with a liquid core is compared in Fig. 2-c, when the effect of gravity is considered. Dots show periods for which the radial distributions of disturbances terminate near the core boundary.

frequency by means of the well-known asymptotic formulae

$$C/V_{S0}=\gamma\Big/\left(n+\frac{1}{2}\right) \tag{6.1}$$

and

$$U/V_{S0}=d\gamma/dn \tag{6.2}$$

Results are graphically represented in Figures 2-a and 2-b. The differences between the phase and group velocities for the present case and those for the case without the influence of gravity are not great except for modes with longer periods and for the radial higher modes $i=1'$. In order to show detailed features of the group velocity curves, a part of the figure is enlarged along the period axis and is given in a rectangular enclosure.

As the period tends toward zero, the phase and group velocities of the fundamental mode approach 0.9194 V_{S0}, corresponding to ordinary Rayleigh waves along a plane boundary. The number of maxima and minima in the group velocity curve increases as the radial mode number i increases. Corresponding maxima and minima seem to lie on smooth curves which tend toward the value $U/V_{S0} \fallingdotseq 1.2$ as the period decreases to zero. A similar feature was pointed out in the case of torsional oscillations of an actual earth model by Satô, Landisman and Ewing[6] and explained in connection with waves which graze the core. Alterman and Kornfeld[7] found the same phenomena for torsional oscillations of an elastic mantle with a liquid core and associated it with a guided wave due to the introduction of the core.

Figure 2-c shows the group velocity for the present case and for the case of a homogeneous gravitating elastic sphere. Broken lines represent the latter case, in which values of maxima and minima approach $U/V_{S0} \fallingdotseq 1.3$ as the period tends toward zero. Dots in the figure correspond to modes for which the displacement becomes negligible near the core boundary ($b/a=0.5447$). Denote the period of these modes by T_i. For modes with periods longer than T_i, the core (or the part of the sphere for which $r<0.5447a$) participates in the free oscillations. The core (or the corresponding part of the solid sphere) does not affect the oscillation for modes with periods shorter than T_i. As may be expected, the group velocities of the two cases for modes with $T<T_i$ do not show any difference.

The maxima and minima of group velocity approach the limit $U/V_{S0} \fallingdotseq 1.3$ for infinitesimally short period spheroidal oscillations of a homogeneous elastic sphere. This limiting velocity is understood by Alterman and Abramovici[8] to be representative of the mixed wave type $P_\mu S_\nu$, in the limit as $\mu \to \infty$. The wave travels μ segments as P and ν segments as S, with multiple reflections at the free surface. This explanation does not seem to be valid, because the limit of the

6) Y. SATÔ, M. LANDISMAN and M. EWING, "Love Waves in a Heterogeneous, Spherical Earth. Part 2. Theoretical Phase and Group Velocities," *J. G. R.*, **65** (1960), 2399-2404.

7) Z. ALTERMAN and P. KORNFELD, "Normal Modes and Rays in the Propagation of a Seismic Pulse from a Point-Source in a Layered Sphere," *Israel Journ. Tech.*, **4** (1966), 198-213.

8) Z. ALTERMAN and F. ABRAMOVICI, "Propagation of a *P*-pulse in a Solid Sphere," *Bull. Seism. Soc. Amer.*, **55** (1965), 821-862.

Z. ALTERMAN and F. ABRAMOVICI, "Effect of Depth of a Point Source on the Motion of the Surface of an Elastic Solid Sphere," *Geophys. J.*, **11** (1966), 189-224.

group velocity maxima and minima, $U/V_{S0} \doteqdot 1.3$, disappears for the case of a homogeneous mantle with a liquid core. The corresponding limit of the maxima and minima for the present case, $U/V_{S0} \doteqdot 1.2$, is caused by the introduction of the core. If they exist in this case, waves corresponding to these extremal values of group velocity seem to be closely connected with the core. Detailed study of these waves will be left for the near future.

7. Common Spectrum

The components of the Common Spectrum, ${}_iS_n{}^u$ and ${}_iS_n{}^v$, for the radial and colatitudinal displacements are defined as

$$\left.\begin{aligned} {}_iS_n{}^u &= \left(\frac{S_{mn}}{dE_S/dp} + \frac{T_{mn}}{dE_T/dp}\right) \cdot U_n(r) \cdot f^*(p) \ , \\ {}_iS_n{}^v &= \left(\frac{S_{mn}}{dE_S/dp} + \frac{T_{mn}}{dE_T/dp}\right) \cdot V_n(r) \cdot f^*(p) \ . \end{aligned}\right\} \tag{7.1}$$

If the temporal and spatial distribution of the applied force is specified, the Common Spectrum is independent of the variables t, θ and φ, and it may be used to calculate the disturbance at all times and locations. Using these expressions, the disturbances may be written

$$\left.\begin{aligned} u(t) &= \frac{j}{2} \sum_{i,m,n} {}_iS_n{}^u \cdot P_n{}^m(\cos\theta) \cdot \begin{matrix}\cos\\ \sin\end{matrix} m\varphi \cdot \exp(jpt) \ , \\ v(t) &= \frac{j}{2} \sum_{i,m,n} {}_iS_n{}^v \cdot \frac{d}{d\theta} P_n{}^m(\cos\theta) \cdot \begin{matrix}\cos\\ \sin\end{matrix} m\varphi \cdot \exp(jpt) \ , \\ w(t) &= \frac{j}{2} \sum_{i,m,n} {}_iS_n{}^v \cdot \frac{mP_n{}^m(\cos\theta)}{\sin\theta} \cdot \begin{matrix}-\sin\\ \cos\end{matrix} m\varphi \cdot \exp(jpt) \ . \end{aligned}\right\} \tag{7.2}$$

The radial and colatitudinal components of the Common Spectrum are shown in Figure 3-a and 3-b. Parts of the figure for small values of n are magnified and given in rectangular enclosures.

The discrepancy between the patterns of the Common Spectrum for the cases with and without the influence of gravity stems from the differences between the constant values defining the temporal and spatial distributions of the applied force. It is remarkable that the maximum value of the Common Spectrum for the fundamental mode is far larger than those for higher radial modes, and that the maximum values of the higher radial modes decrease rather gradually as the mode number i increases. This gradual decrease implies that the

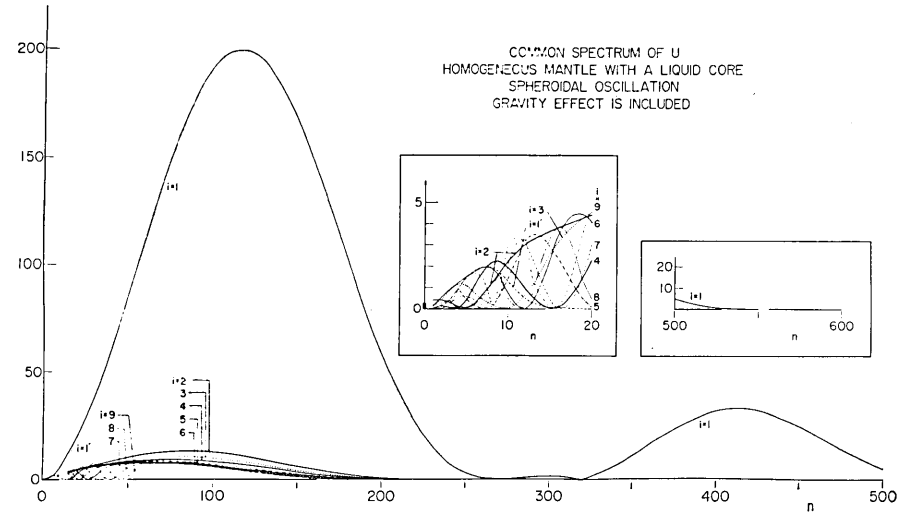

Fig. 3-a.

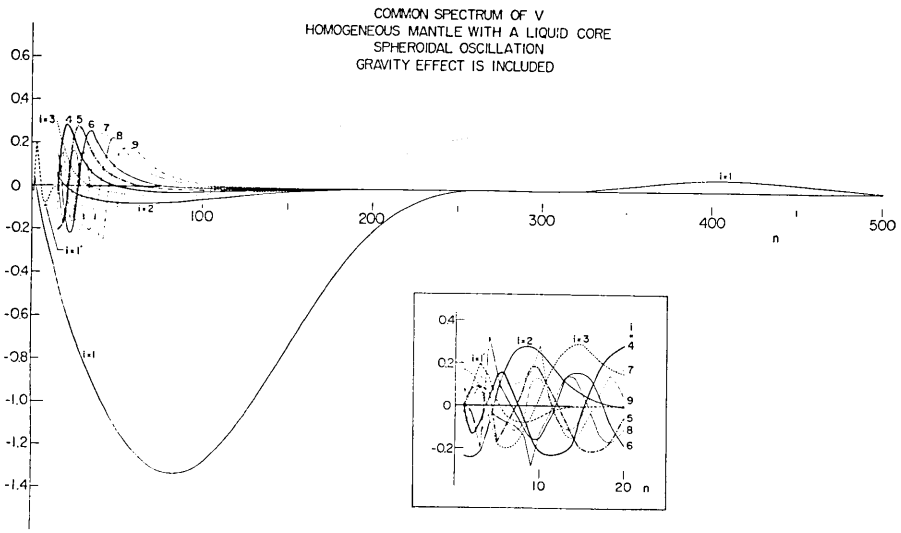

Fig. 3-b.

Fig. 3. Common Spectrum of radial and colatitudinal components of displacement. Portions of these curves for large and small values of n are enlarged in enclosures. Values of radial component for $n=0$ are given by dots.

addition of radial higher modes with $i>9$ will improve the accuracy of the theoretical seismograms which express the body waves. The effect of this improvement will be discussed in the near future.

The Common Spectrum decreases as the colatitudinal order number

n increases. It becomes negligibly small when n is larger than 500 for the fundamental mode, and for values in excess of 250 for the higher radial modes.

8. Theoretical Seismograms

A purely radial stress is applied to a small circular area around the pole, implying axial symmetry ($m=0$). Its geographical distribution is

$$\Phi(\theta,\varphi)=\Phi^0(\cos\theta)=\begin{cases}1 & \theta<\theta_0\\ 0 & \theta_0<\theta\end{cases}\quad(\theta_0=0.012 \text{ radian})\ . \tag{8.1}$$

The time function is taken to be

$$f(t)=\begin{cases}-1 & -t_1<t<0\\ 1 & 0<t<t_1\\ 0 & |t|>t_1\end{cases}\quad(t_1=0.004)\ . \tag{8.2}$$

From the function given above, the Fourier transform is immediately given as

$$f^*(p)=-4j\sin^2(pt_1/2)/p\ . \tag{8.3}$$

The largest values of colatitudinal order number n employed in the synthesis are

i	1	1′	2	3	4	5	6	7	8	9
$n_{\max}$	540	37	481	470	460	452	445	439	432	429

Theoretical seismograms are calculated at 11 points on the surface, namely $\theta=15°(15°)165°$ for the time interval $t=0.001(0.001)1.000$. The time required for the S wave to circle the sphere ($2\pi a/V_{S0}$) is taken as the unit. The seismograms are shown in Figures 4-a, 4-b, 5-a, 5-b and 7.

In Figure 4-a, the solid line shows (${}_9u_{600}$) and (${}_9v_{600}$) and the broken line (${}_1u_{600}$) and (${}_1v_{600}$). The expected arrival time of various body waves as predicted by geometrical optics is indicated in the figure. Figure 4-b shows theoretical seismograms consisting of contributions from radial higher modes. These figures imply that the fundamental mode is closely related to the surface waves, while the radial higher modes are associated with the body waves. The agreement between the expected times of arrival and the actual times of appearance of the body phases is satisfactory.

The Rayleigh wave shows characteristic features. The disturbance

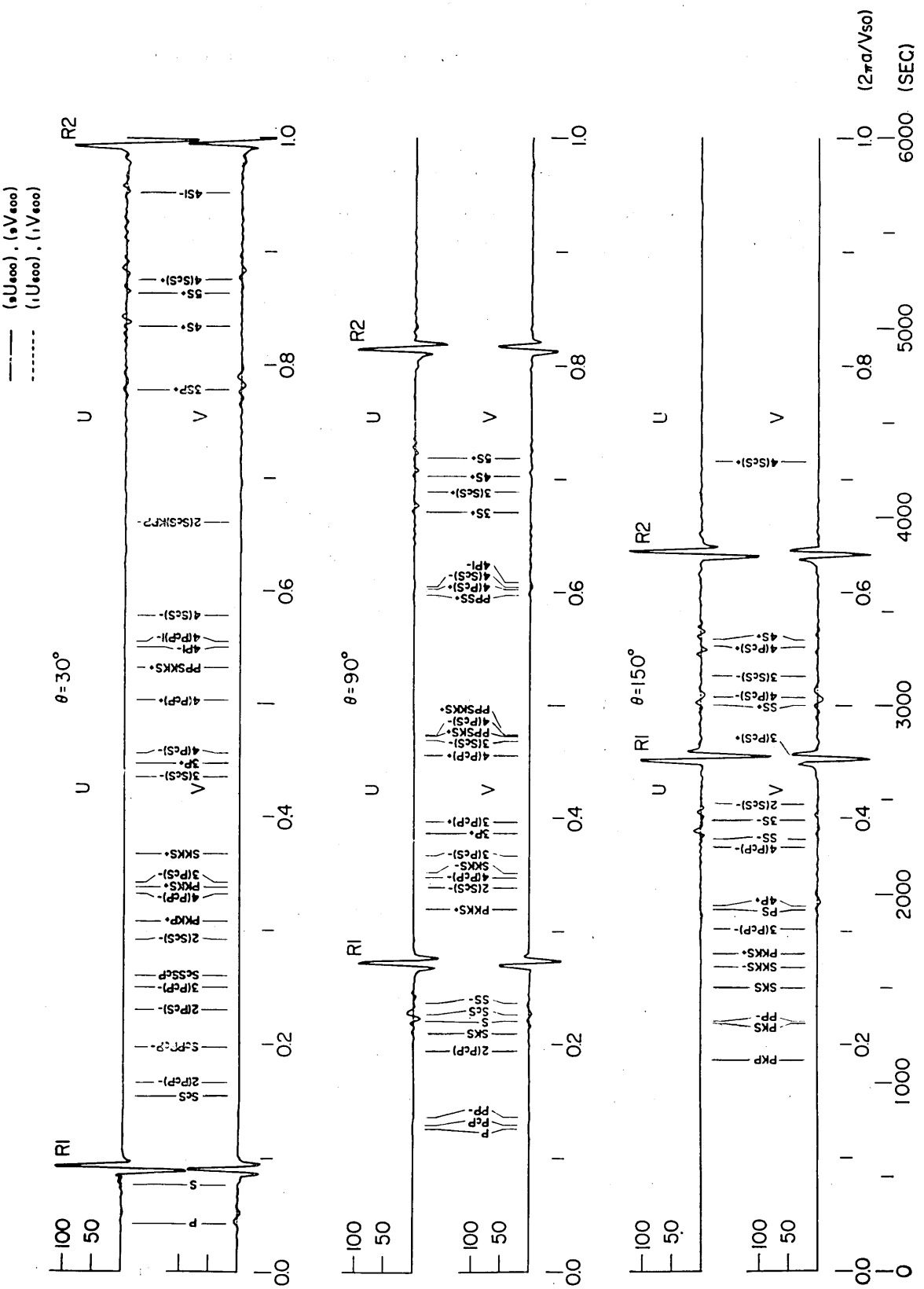

Fig. 4-a.

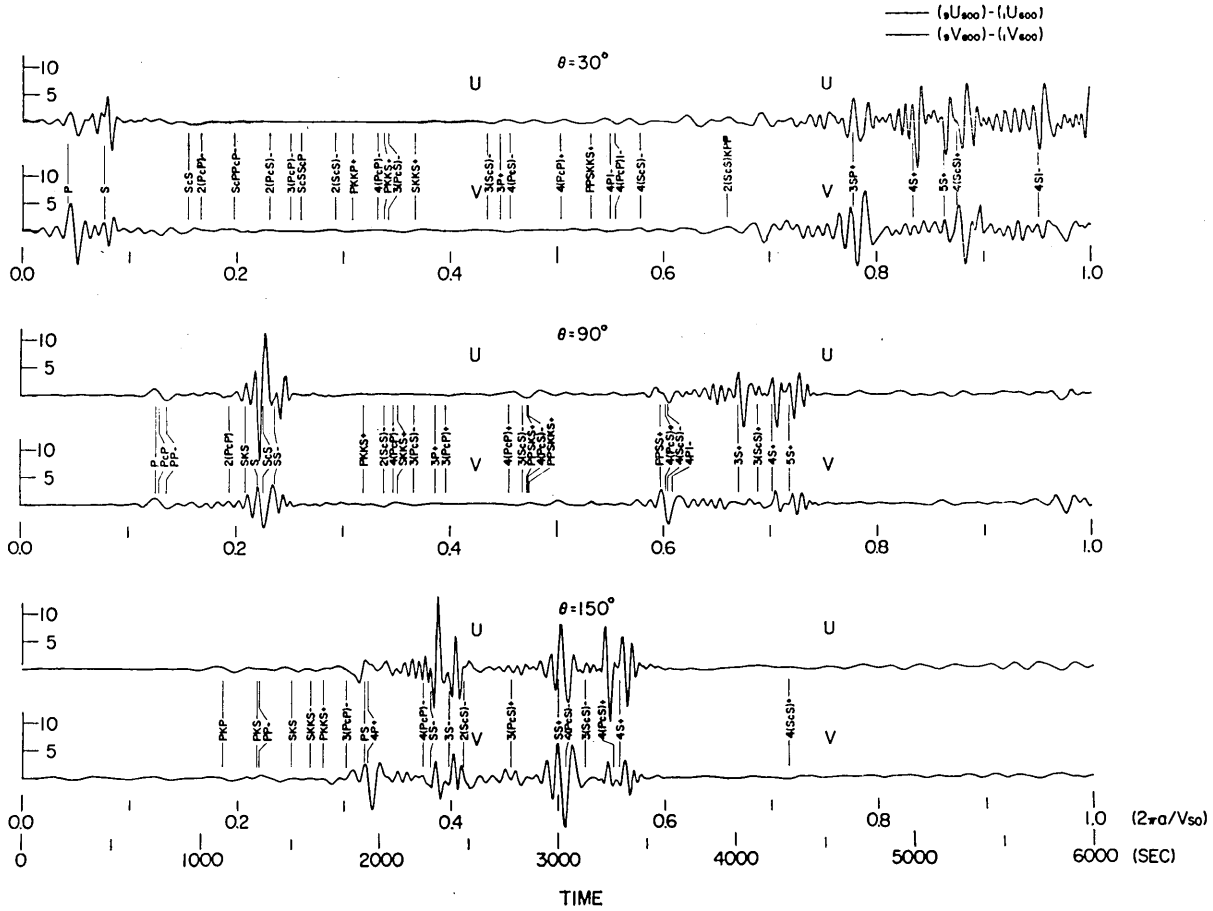

Fig. 4-b.

Fig. 4. Theoretical seismograms of spheroidal disturbances on the surface of a gravitating elastic sphere with a homogeneous mantle and a liquid core. A purely radial force is applied to a small circle around the pole. Solid lines: $({}_9u_{600})$, $({}_9v_{600})$. Broken lines: $({}_1u_{600})$, $({}_1v_{600})$. Arrows show the arrivals of various body phases calculated by geometrical optics. Unit of time: $2\pi a/Vs_0$. The difference between solid and broken lines, that is the sum of contributions from only the radial higher modes, is shown in magnified scale in Fig. 4-b. The higher modes show the arrival of body phases more clearly. Fig. 4-a is reproduced from our preliminary report[5].

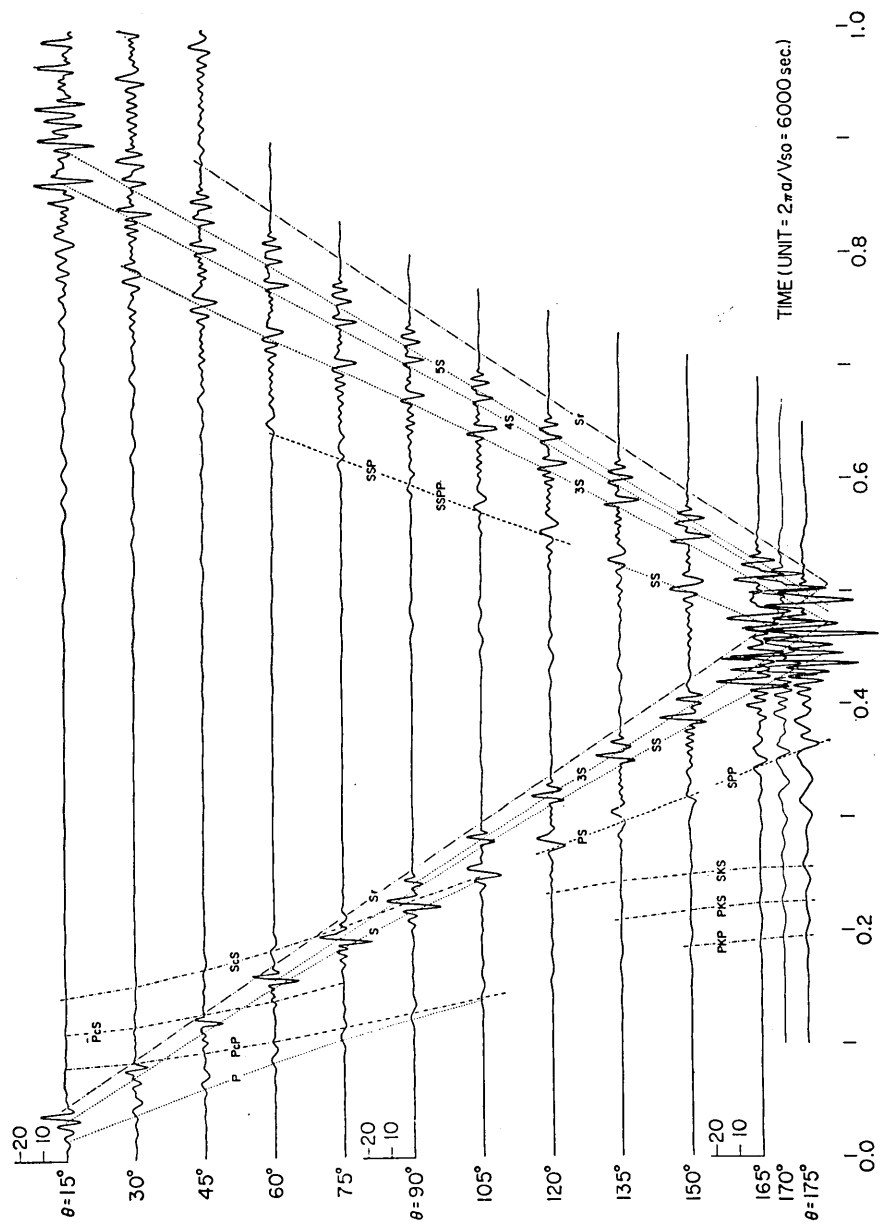
θ=15°
30°
45°
60°
75°
θ=90°
105°
120°
135°
150°
165°
170°
θ=175°
20
10
P
PcP
PcS
ScS
S
Sr
SSP
SSPP
5S
4S
3S
SS
PKP
PKS
SKS
SPP
TIME (UNIT = 2πa/Vso = 6000 sec.)
0.0
0.2
0.4
0.6
0.8
1.0

Fig. 5-a.

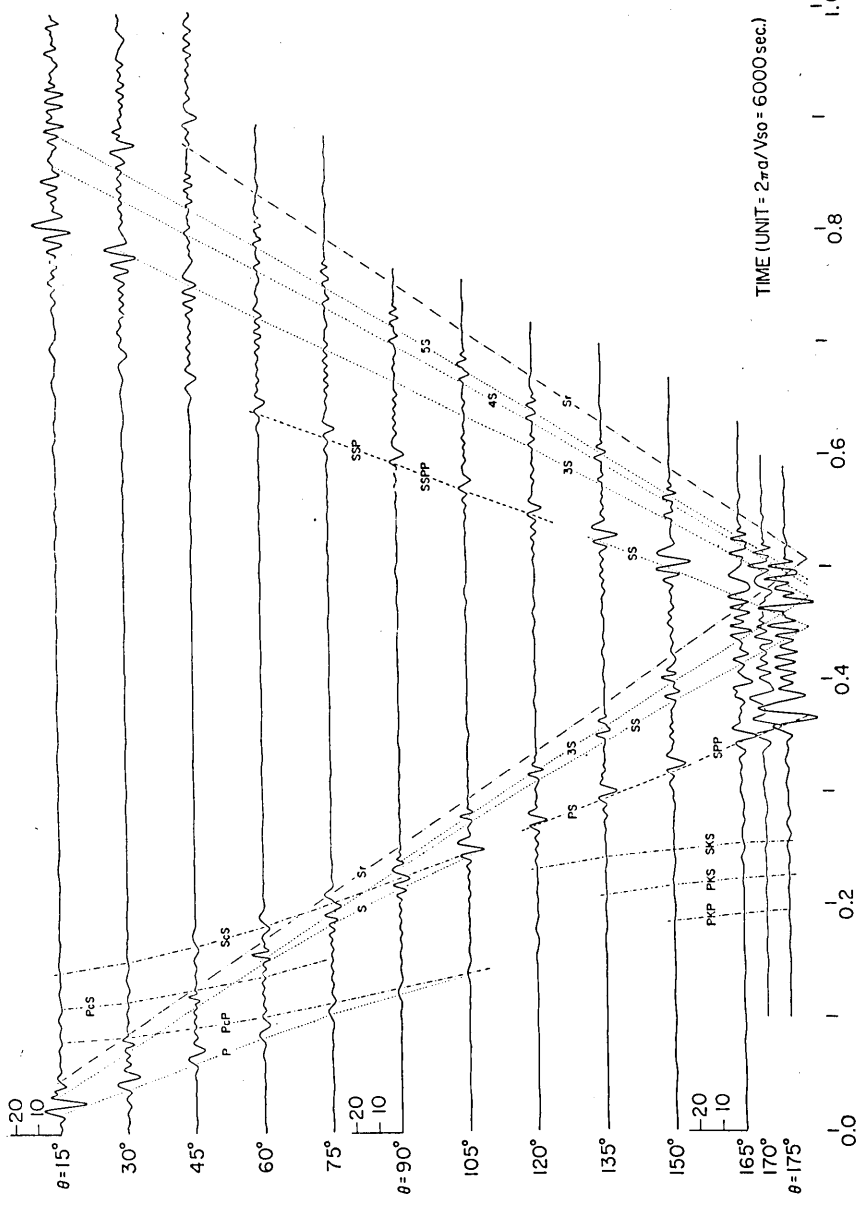

Fig. 5-b.

Fig. 5. Radial and colatitudinal displacements computed for various epicentral distances. The curves show the contribution from only radial higher modes. Various kinds of broken lines indicate travel time curves of body phases. Splitting of S wave into multiply-surface-reflected waves can be traced on the theoretical seismograms. S_r is the travel time of a wave propagated along the surface with the shear wave velocity. Fig. 5-a shows radial component, and Fig. 5-b shows colatitudinal component.

continues for nearly one cycle and has a phase which changes gradually with epicentral distance. Its apparent period, nearly 60 sec, reflects the period of the applied force, 48 sec. Theoretical seismograms of the Rayleigh wave will be analysed and discussed in detail in the next section. Figures 5-a and 5-b are the theoretical seismograms showing the disturbances of radial higher modes, calculated at points with epicentral distances $\theta=15(15)165°$. The curves clearly represent the propagation of the body waves. The direct waves, surface-reflected waves and waves reflected at and diffracted by the core can be identified on the seismograms. The splitting of the S wave into multiply- surface-reflected S waves such as SS, SSS, $\cdots$ with increasing epicentral distance, is well represented on the seismogram. The phase change of π between the S wave reflected n times and $(n+2)$ times at the surface[9] is also seen in the seismograms.

Figure 6 shows the variation of total amplitude of body waves read from the theoretical seismograms in Figures 5-a and 5-b. Curves representing the variation of amplitude as a function of epicentral distance are calculated from the divergence factor after taking the effect of reflection at the surface into account[10]. The reflection coefficient is

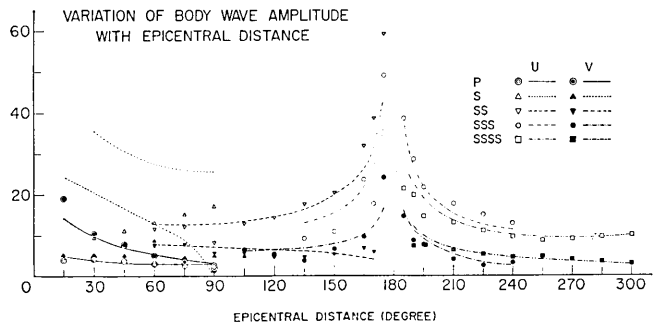

Fig. 6. Variation of radial and colatitudinal components of amplitude of various body waves read from seismograms in Fig. 5 as a function of epicentral distance. Curves show theoretical values calculated from the divergence factor, taking into account the reflection at the free surface. Ordinate scale for observed values is consistent with that of Fig. 5. Ordinate scales for calculated curves are adjusted by multiplicative factor. This factor is same for S, SS, SSS and $SSSS$ waves, and a different factor is adopted for P wave.

9) H. SHIMAMURA and R. SATO, "Model Experiments on Body Waves—Travel Times, Amplitudes, Wave Forms and Attenuation," *Journ. Phys. Earth*, **13** (1965), 10-33.

10) M. LANDISMAN, Y. SATÔ and T. USAMI, "Propagation of Disturbances in a Gutenberg-Bullen A′ Spherical Earth Model: Travel Times and Amplitudes of S Waves," *Amer. Geophy. Union, Monog.* **10**, J.S. Steinhart and T.J.Smith, eds., (1966), 482-494.

obtained by assuming a plane P or SV wave incident upon a plane free surface. The scale of the ordinate is the same as that of Figure 5. Curves are adjusted by a constant multiplier for the S, SS, SSS and $SSSS$ waves. A different constant is adopted for the P wave. Satisfactory coincidence is obtained between the curves and the observed values. For each wave, better agreement is found at epicentral distances where the waves are isolated and well developed.

Figure 7 shows the displacements obtained by summing up the contributions from the first several radial higher modes. Waves which travel most of their paths with the velocity of S waves may be expressed by the summation of contributions from the comparatively lower order overtones, while contributions from higher order overtones are necessary in order to express the P wave group. Comparison of Figure 7 with the corresponding figure for the case without the effect of gravity[4], shows that near the arrival of the S wave group the convergence of the sum of radial higher modes is not so rapid in the present case as in the case excluding the effect of gravity. This indicates that the neglected radial higher modes should make an appreciable contribution to the total disturbance. Figures of the Common Spectrum also show these features.

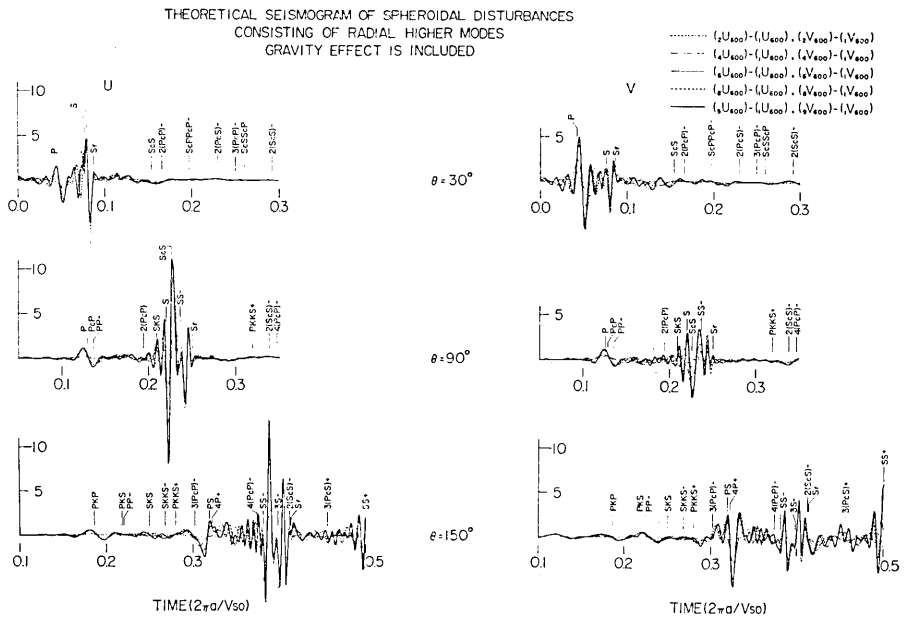

Fig. 7. Theoretical seismograms showing contributions of radial higher modes to various kinds of body waves. The meaning of each line is given in the figure.

The notation S_r in Figure 7 refers to the theoretical arrival time of an S wave reflected an infinite number of times at the surface, which is equivalent to the time required for an S wave to travel to the station along the surface. Disturbances due to the S wave group end abruptly near this time S_r.

In terms of ray theory and its observed travel time, the wave S_r may be considered to be an S wave reflected an infinite number of times at the free surface. The period of S_r in Figure 7 is found to be about 0.01 unit ($\fallingdotseq$60 sec). For this period range, the group velocities of the radial higher modes are in the range $U/V_{S0}=1.02\sim1.15$ and show monotonous features as functions of period. The summation of contributions from these modes will explain the S_r wave in terms of normal mode theory. The difference between the travel time of S_r and the end point of the S wave group in Figure 5 can be explained by the group velocity of the radial higher modes for periods near 60 seconds. This group velocity is slightly larger than V_{S0}. For the non-gravitating case[4], the period of the applied force is 240 seconds. The group velocities for that case show sharp variations for periods near 240 seconds. There are also sizable differences between the values for the various radial higher modes; consequently the S_r wave can not be identified on theoretical seismograms consisting of radial higher modes in that case. From its apparent velocity, V_{S0}, Alterman and Kornfeld[7] explain the S_r wave for the torsional oscillation as a surface wave of limiting group velocity $U=V_{S0}$. In the present case, the S_r wave represents contributions from the short period portions of the higher radial mode dispersion curves. Reference to the group velocities in Figure 2-b, the components of the Common Spectrum in Figure 3 and later portions of the seismograms in Figure 5 shows that the well excited regions of these overtones produce a number of surface reflections. At first these reflections grow in number with increasing travel time. They then wane as the time corresponding to S_r approaches because the extremely short period portions of these overtones are not well excited by the present source function. A source function with a shorter time duration should excite multiple reflections which more closely approach the limit defined by S_r.

9. Analysis of Rayleigh Waves

The Rayleigh waves show characteristic features including a sudden commencement followed by a disturbance which lasts for about 90 sec

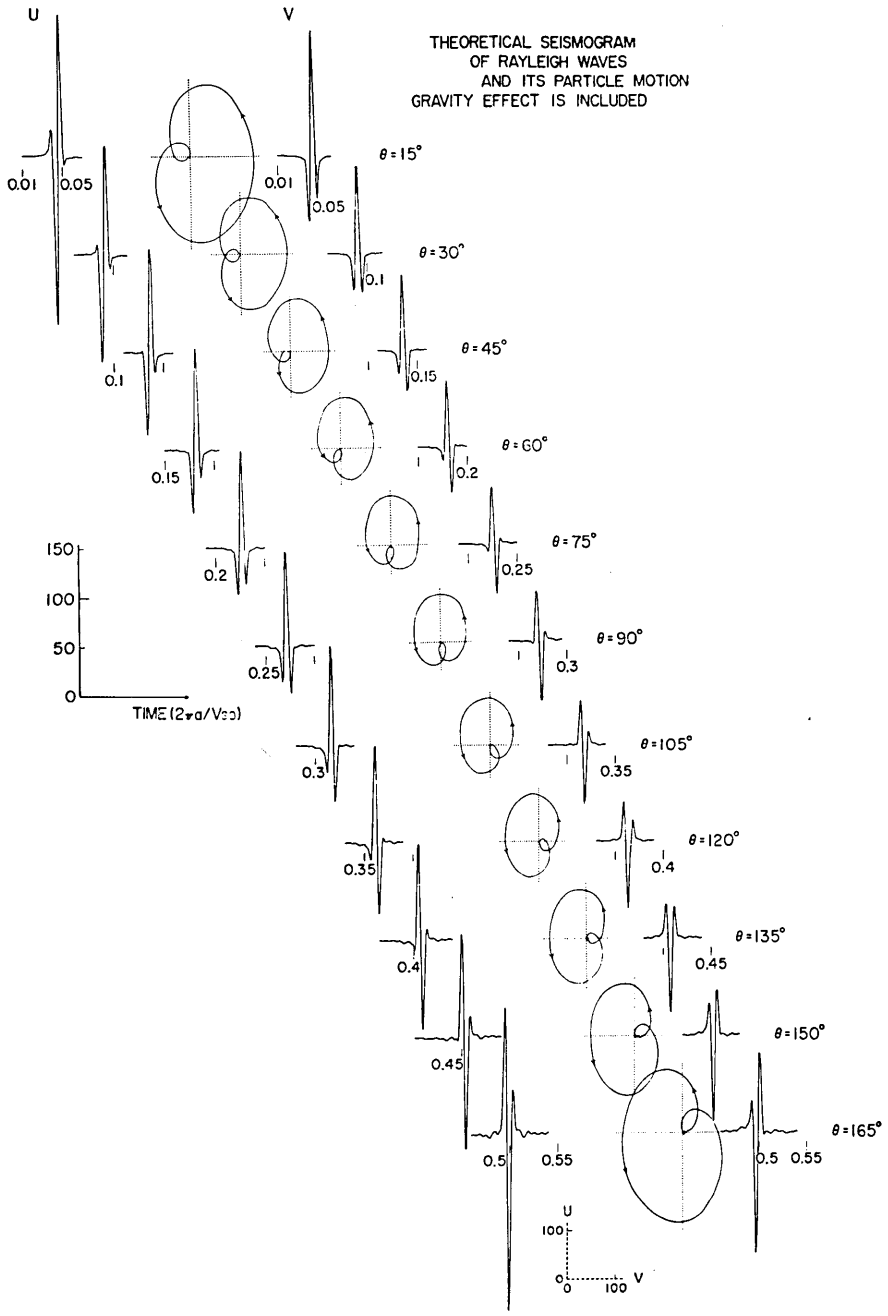
U
V
THEORETICAL SEISMOGRAM
OF RAYLEIGH WAVES
AND ITS PARTICLE MOTION
GRAVITY EFFECT IS INCLUDED
θ=15°
θ=30°
θ=45°
θ=60°
θ=75°
θ=90°
θ=105°
θ=120°
θ=135°
θ=150°
θ=165°
0.01
0.05
0.1
0.15
0.2
0.25
0.3
0.35
0.4
0.45
0.5
0.55
150
100
50
0
TIME (2πa/V₀)
U
100
0
0
100
V

Fig. 8-a.

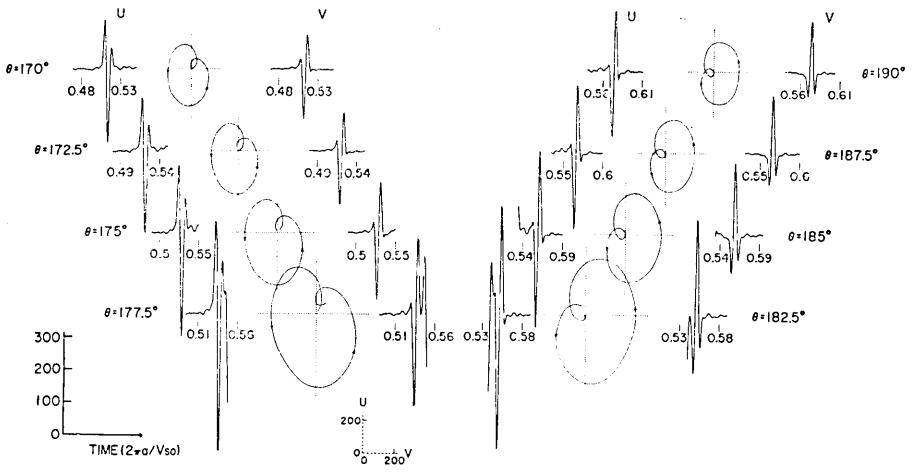

Fig. 8-b.

Fig. 8 Theoretical seismograms of Rayleigh waves and the orbit of particle motion. Scale of orbital motion is half as large as those for radial and colatitudinal components. Orbit shows elliptic form. Ratio of vertical to horizontal axes is nearly equal to 1.46, corresponding to Rayleigh waves along a plane boundary.

and ends abruptly. The period is about 60 sec corresponding to the 48 sec period of application of the theoretical generating force. Figures 8-a and 8-b show the Rayleigh waves consisting of contributions from only the fundamental radial mode. The orbit of particle motion exhibits typical characteristics of Rayleigh waves: 1) elliptical form, 2) retrograde particle motion, 3) amplitude ratio of the vertical and horizontal displacement which is nearly equal to the theoretical value of 1.46 for a Rayleigh wave along the plane bounding a homogeneous half-space with the physical properties of the outer shell.

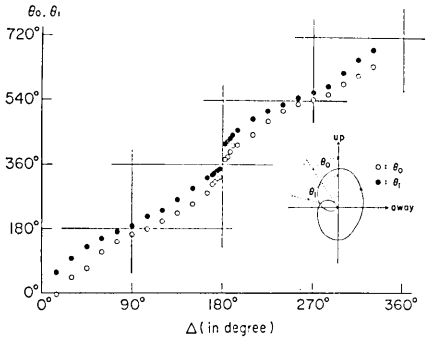

Fig. 9. Graph showing the change of angles θ_0 and θ_1 as functions of epicentral distance. The meaning of these angles is explained in the figure. They show sudden change of about $\pi/2$ near the antipode, indicating polar phase shift in orbital motion.

The amplitude of the Rayleigh wave becomes large near the pole and the antipode, which is a characteristic of surface waves propagating on a spherical surface. In Figure 9 the angle θ_0, between the vertical line and the tangent to the orbital motion of the Rayleigh wave at its start, is considered to be closely related to the

phase of the wave since in the present case the Rayleigh wave has a sharp onset. The variation of this angle as a function of epicentral distance shows a sudden change near the antipode which amounts to $\pi/2$, the value corresponding to the polar phase shift. This phenomenon may be explained as follows. When n is large

$$\left.\begin{aligned} u &\propto \cos\left\{\left(n+\frac{1}{2}\right)\theta-\frac{\pi}{4}\right\} \\ v &\propto \cos\left\{\left(n+\frac{1}{2}\right)\theta+\frac{\pi}{4}\right\} . \end{aligned}\right\} \tag{9.1}$$

The phase difference between the u- and v-components of displacement is

$$\varphi_c=\varphi_u-\varphi_v=\left[\left(n+\frac{1}{2}\right)\theta-\frac{\pi}{4}\right]-\left[\left(n+\frac{1}{2}\right)\theta+\frac{\pi}{4}\right]=-\frac{\pi}{2} . \tag{9.2}$$

Upon passing the antipode, the radial and colatitudinal displacements are subjected to polar phase shifts of $-\pi/2$ and $\pi/2$ respectively. Considering the reversal of the relation between the direction of propagation and the plus direction of the colatitudinal coordinate θ at two points, close to and on opposite sides of the antipode or pole, the polar phase shift of the colatitudinal component is finally

$$\frac{\pi}{2}+\pi=\frac{3}{2}\pi \Longrightarrow -\frac{\pi}{2} . \tag{9.3}$$

The phase difference φ_c, after passing the antipode is

$$\varphi_c=\varphi_u-\varphi_v=\left[\left(n+\frac{1}{2}\right)\theta-\frac{\pi}{4}-\frac{\pi}{2}\right]-\left[\left(n+\frac{1}{2}\right)\theta+\frac{\pi}{4}+\frac{\pi}{2}+\pi\right]=-\frac{\pi}{2} . \tag{9.4}$$

Formulae (9.3) and (9.4) indicate that the phase shift of both components is the same, namely $-\pi/2$. This explains the sudden change of angle $\theta_0=\pi/2$ near the antipode and the conservation of the three characteristics of the Rayleigh wave as given above, at places close to and on opposite sides of the antipode.

The theoretical disturbance of the Rayleigh wave was calculated by summing up contributions from a large number of component waves with different spectral amplitudes and different phase velocities. Therefore, the synthesized wave form could be explained by the terminology of dispersion, although the wave form does not show any apparent dispersive character such as the period change with arrival

time[11]. In order to show these points vividly, numerical analysis was performed, regarding the theoretical seismograms as observed recordings. The method of Fourier analysis was applied and the Fourier spectrum, the initial phase β, omitting the effect of the polar phase

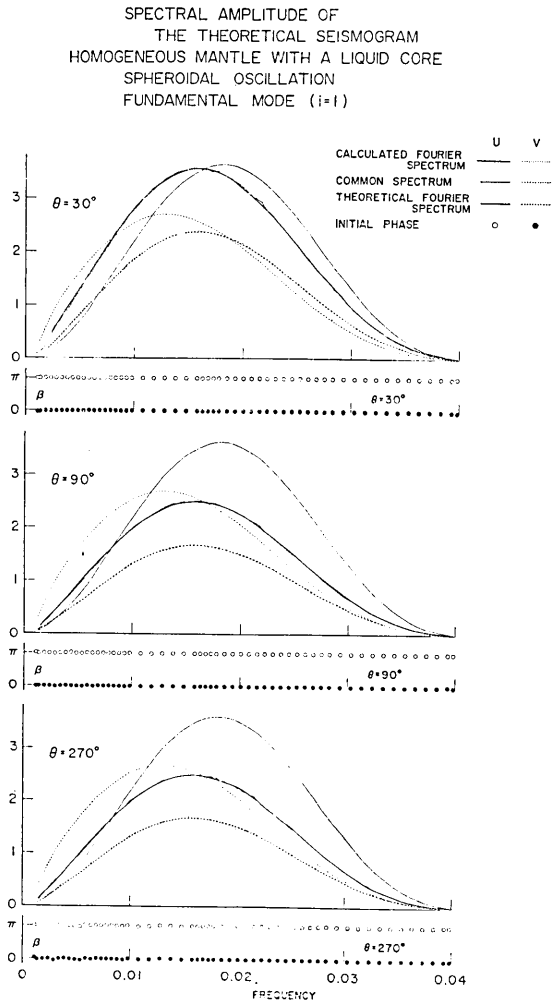

Fig. 10. Fourier spectrum and initial phase β calculated from theoretical disturbance of the fundamental mode. Agreement between the theoretical and calculated spectra is satisfactory. The effect of polar phase shift has been removed from the initial phase. Open circle refers to radial component and solid circle to colatitudinal component.

11) Y. SATÔ, "Attenuation, Dispersion, and the Wave Guide of the *G* Wave," *Bull. Seism. Soc. Amer.*, **48** (1958), 231-251.

shift, and the phase velocity were calculated. They are shown in Figures 10 and 11.

In Figure 10, thick solid and thick broken lines show the envelope of curves given by $|{}_iS_n^u \cdot P_n(\cos\theta)|$ and $\left|{}_iS_n^v \cdot \frac{d}{d\theta}P_n(\cos\theta)\right|$ respectively. The value π of the initial phase β for the radial component stems from the minus sign in expression (8.3), and the value zero for the colatitudinal component is the combined effect of this sign and the sign of $(v/u)_{r=a}$, which is negative for all orders when $i=1$. The remarkable agreement between these calculated quantities and the theoretical ones shows that wave propagation with no apparent change of period can be explained by the concept of dispersion.

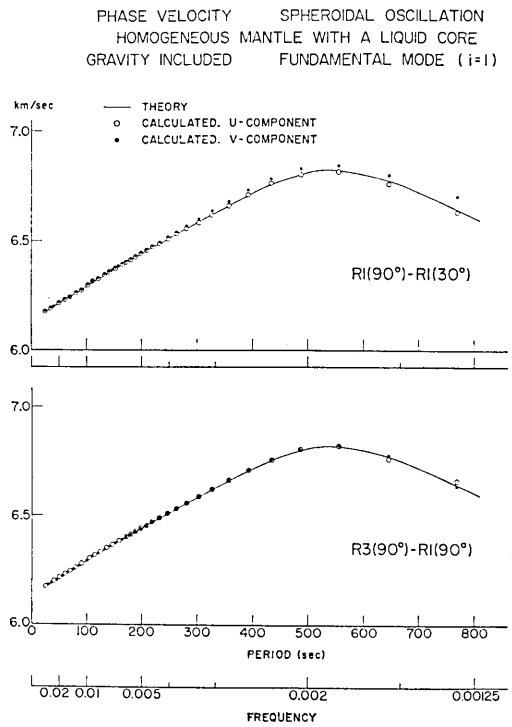

Fig. 11. Phase velocity calculated by the method of Fourier analysis from theoretical seismograms of fundamental mode. Open and solid circles refer to the radial and colatitudinal components respectively. These circles lie on the solid line expressing phase velocity calculated by equation (6.1) from theoretical values of non-dimensional frequency.

Acknowledgement

The authors are greatly indebted to Professor Max Goldstein,

Director of the computing laboratory of the Courant Institute of Mathematical Sciences, New York University, for his generous hospitality and provision of computing facilities, under the auspices of U.S. Atomic Energy Commission contract AT-(30-1)-14800 and AT-(40-1)-3708. Parts of the computation were done through the project UNICON, and at the Computer Centre of the University of Tokyo, to all of whom our sincere thanks are due.

The authors are grateful to the Geosciences Division of the Southwest Center for Advanced Studies and the Earthquake Research Institute of the University of Tokyo for their help in arranging a visit of Y. Satô to the former institution while on leave from the latter during the period of this study.

This cooperative research in the field of seismology was supported in part by the Japan Society for the Promotion of Science and the National Science Foundation under grants Chi-26 and GF-237, respectively, as part of the Japan-U.S. Cooperative Science Program. This investigation was also supported by the National Science Foundation under grants GA-830 and GA-1404, by the National Aeronautics and Space Administration, under contract NsG-269-62 with Southwest Center for Advanced Studies and by supplemental research funds of the latter institution.

---

38. 重力均衡下にある弾性球の表面を伝わるスフェロイド型振動 III. 流体核をもつ等方等質マントルの場合

地震研究所 宇佐美龍夫
地震研究所 佐藤泰夫
Southwest Center for Advanced Studies Mark LANDISMAN
東京大学・大学院 小高俊一

1. 我々は弾性球の自由振動周期や理論地震記象に及ぼす重力の影響を研究して来たが，その第3報として，流体核のある等方等質マントルの場合のスフェロイド型振動の理論地震記象を作つた．方法は従来と同じで，変位をいろいろな固有振動のモードの和として表わした．

2. 弾性球モデルとしては重力のない場合と同じものを採用した．しかし重力を考慮に入れると，核とマントルの密度比のみでなく，密度の値そのものも与えないと固有振動はきまらない．ここでは $\rho_i=10.171$, $\rho_0=4.6232$ とした．したがつて弾性球の平均密度は $5.52\,\mathrm{gr/cm^3}$ となる．

3. スフェロイド型の自由振動の周波数を，$i=1(1)9$ に対し，12秒以上の周期をもつすべてのモードについて求めた．n の最大値は $i=1$ のときに 541 である．重力の影響は長周期の振動に大きく，周期が短かくなると無視しうる．とくに $i=1'$ というモード（核の境界を伝わるストンレー波に相当する）に対する影響が大きい．

4. 群速度と位相速度に及ぼす重力の影響は周波数に対する影響を強く反映して $i=1\sim3$ のモードのうち周期の長いものに対して大きい．高調波の群速度に現われる極大・極小の数は i とともに増加し，互に対応する極値を結ぶと周期の小さくなる極限で $U/Vs_0\to1.2$ ca. となる．これに反し，等質等方弾性球の時には $U/Vs_0\to1.3$ ca. となる．このことから等質等方弾性球の場合に，この極値を表面で多数回反射をする実体波と解釈した Alterman らの試みは妥当でないことが分かる．なお，核が関与しないような短周期モードの群速度は，等質等方弾性体の場合と，本論文の場合とは完全に一致する．

5. 従来にならつてコモン・スペクトルを計算した．これは外力の関数である．今回は短周期モードまで考えたために，重力のない場合と異なる外力を採用したので，重力のない場合と比べることはできない．基準モードに比し高調波のスペクトル振幅は遙かに小さい．また高調波スペクトルの極大値は i の増加につれて徐々に減少する．

6. 数値計算に当り，軸対称 $(m=0)$ を仮定した．外力としては極のまわりに次のような半径方向の力が働くとした．

$$\Phi(\theta,\varphi)=\Phi^0(\cos\theta)=\begin{cases}1 & \theta<\theta_0\\ 0 & \theta_0<\theta\end{cases}\quad(\theta_0=0.012\ \text{ラヂアン})$$

$$f(t)=\begin{cases}-1 & -t_1<t<0\\ 1 & 0<t<t_1\\ 0 & t_1<|t|\end{cases}\quad(t_1=0.004)$$

時間の単位としては (周長)/(地表の S 波速度)=6000 秒 をとり，弾性球上の数点で $t=0.001(0.001)1.000$ について理論地震記象を計算した．

7. 計算の結果，次のことが明らかになつた．

a) 基準振動は表面波をよく現わし，高次振動は実体波と密接に関係する．

b) 幾何光学的に求められた実体波の走時は，理論地震記象上に現われる波の発現時とよい一致を示す．

c) 短周期波に着目すると，群速度の極小値に対応して表面波の終わりの点がはつきり理論地震記象上に見出される．

d) 高調波からなる理論地震記象上にはつきりみられる P, S, SS, $3S$, $4S$ 波の振幅の震央距離による変化の様子は，理論曲線 (波の幾何学的拡散と，地表面における平面波としての反射の効果を考えたもの) とよく一致する．

e) レイリー波は始まりと終わりのはつきりしたパルス型の振動を示す．一見，分散性を示さないが，分散波として完全に説明できることが，解析の結果分かつた．また，粒子運動の軌跡をかくと，平面境界におけるレイリー波の性質を示している．レイリー波の始点においてこの軌跡に接線を引くと，その接線の向きは震央距離とともに変化し，対極点をはさんで $\pi/2$ だけ急変する．これは極での位相のずれが軌跡に発現したものとして説明出きる．

f) 高次振動を加え合わせた理論地震記象上に，表面で多数回反射する S 波の終わりの点がはつきり認められる．これは波線理論的に考えると，表面で無限回反射する S 波に当る．

一方，その波の周期と，群速度の図を参照すると，モード理論的には，群速度が Vs_0 に近い，高次振動の重ね合わせとして理解される．